University of Tabriz

Journal of Civil and Environmental Engineering

Experimental Study and Finite Elements of BRBF for AISC 341-16

Hedayat Veladi [a,*], Bahman Farahmand Azar [b], Omid Ghashang Pour [c], Erfan Yahyazad [d]

[a] *Associate Professor of Structural Engineering, Department of Structural Engineering, Faculty of Civil Engineering, University of Tabriz, Tabriz 5166616471, Iran*

[b] *Professor of Structural Engineering, Department of Structural Engineering, Faculty of Civil Engineering, University of Tabriz, Tabriz 5166616471, Iran*

[c] *M.Sc. Student of Structural Engineer, Department of Structural Engineering, Faculty of Civil Engineering, University of Tabriz, Tabriz 5166616471, Iran*

[d] *Ph.D. Student of Structural Engineer, Department of Structural Engineering, Faculty of Civil Engineering, University of Tabriz, Tabriz 5166616471, Iran*

Received 29 October 2023, Received in revised form 05 December 2023, Accepted 10 December 2023

ABSTRACT:

After the Northridge earthquake, special concentrically braced frames (SCBF) have recently been introduced; further studies conducted to eliminate their shortcomings, design flaws and implementation of connector plates and their vague behavior after seismic load cycles led to development of a new CBF called buckling restrained braced frame (BRBF). In these braces, the steel core which is enclosed within steel profile filled by special concrete encloses the core completely and prevents buckling and increased critical load until compressive axial capacity is only restrained by steel yield tension. This allows the steel core resist against axial forces using entire resistance of the steel as long as casing resists against tensile buckling. As a result, braces act as structural fuse and lead to plastic behaviors, beams, and columns remain elastic in the seismic process. This study builds, tests and numerically models a buckling restrained brace to evaluate sample adequacy to meet requirements of the AISC 341-16 code.

KEYWORDS:

Buckling restrained brace, Buckling restrained braced frame, Ductility.

1. Introduction

Structural bracing systems, shear wall, moment frame, and dual or mixed systems are various types of seismic resistant systems which have been considered and used by design engineers.

In recent earthquakes, severe damages to convergent braces resulting from lack of suitable ductility prove the necessity to review the design of these systems. After the Northridge earthquake, special concentrically braced frames (SCBFs) have recently been introduced; further studies conducted to eliminate their shortcomings, particularly those related to compressive buckling, design flaws and implementation of connector plates and their vague behavior after seismic load cycles led to development of a new CBF called bucking restrained braced frame (BRBF).

(Sabelli et al, 2003) studied 3 and 6-story buildings using nonlinear dynamic analysis and found that BRBFs modify most problems of CBFs such as brace buckling and unbalanced force on the beam center. Moreover, BRBF response was more predictable and relatively better than previous studies on SCBFs and even SMRFs.

In 2004, a real-scale experiment done in Berkeley University showed weak non-elastic performance of SCBF due to its intrinsic buckling behavior, while laboratory results showed good performance of BRBF system compared with SCBF system.

In 1988, BRB system was first used with moment frames in Japan due to considerable energy dissipation; since 2000, it has been widely used as

Publisher: Vice Chancellery for Research & Technology, University of Tabriz
DOI: 10.22034/JCEE.2023.59023.2295
Online ISSN: 2717-4077
* Corresponding Author
E-mail addresses: hveladi@tabrizu.ac.ir (Hedayat Veladi), b-farahmand@tabrizu.ac.ir (Bahman Farahmand Azar), omid_gh22@yahoo.com (Omid Ghashang Pour), erfan_yahyazadeh@tabrizu.ac.ir (Erfan Yahyazad).

damper in high-rise buildings in Japan.

Since 2005, design requirements of BRBF system were included in international regulations such as AISC 341; currently, hundreds of projects are done worldwide using this system.

Not only BRB is used in BRBF, this brace is used in moment frames to control drift due to its predictable behavior. Moreover, BRBF is used with special steel moment frame.

2. Lateral Load Resisting System

Generally, a simple frame system is a structure in which vertical loads are borne by spatial frames and lateral loads are borne by shear walls or braced frames. Braced frame system is one of the first systems resisting against lateral forces. General configuration of braces includes concentrically braced frame (CBF) and eccentrically braced frame (EBF). Buckling restrained braced frame (BRBF) is a special type of CBF.

3. Buckling Restrained Braced System

Buckling restrained braces are formed of a narrow steel core for resisting against axial forces; this yielding part provides its optimally ductile, balanced behavior. Moreover, a casing surrounds the core consistently to prevent its buckling under compressive axial force. A free distance separates steel core and casing to prevent force exchange between them. There are various types of BRB systems based on different forms of steel core and casing to achieve BRB performance.

3.1. Elements of buckling restrained brace

Casing: BRB casing may be rectangular, square or round to provide architectural conditions and to control structural behavior. Casing is mainly responsible for preventing full buckling of the steel core.

Steel core: steel core is fully enclosed within the casing filled by special concrete; therefore, buckling is prevented and critical load is so increased that compressive axial capacity is only restrained by steel yield tension.

Bond-preventing layer: a free distance between steel core and casing separates them to prevent force exchange. For this distance, materials with low friction coefficient such as Teflon, polystyrene and similar materials known as bond-preventing layer are used. This free distance guarantees the space required for steel core expansion under the effect of Poisson phenomenon; however, this distance is not too long to cause local buckling of steel core.

Note that, a stable collar end design is used at the end of the casing to eliminate the need for full penetrating welding. This improves load transmission path and allows visual inspection after seismic events. Fig. 1 shows the details of BRBFs.

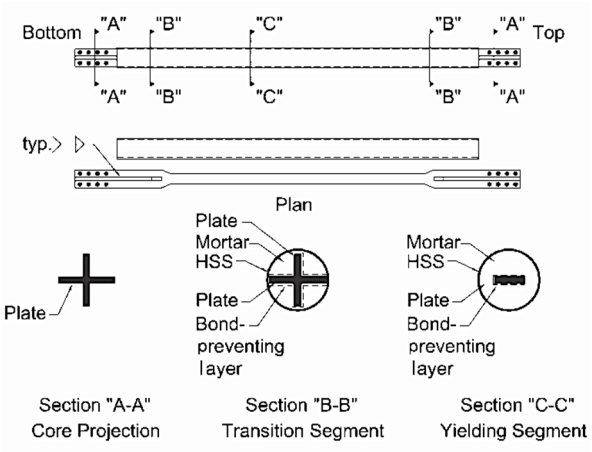

Fig. 1. Details of buckling restrained brace (courtesy of R. Tremblay) [AISC 341-16]

Different BRBF configurations are single diagonal or zigzag. Obviously, they cannot pass through or intersect each other because of the nature of this brace. Fig. 2 shows different BRBF configurations.

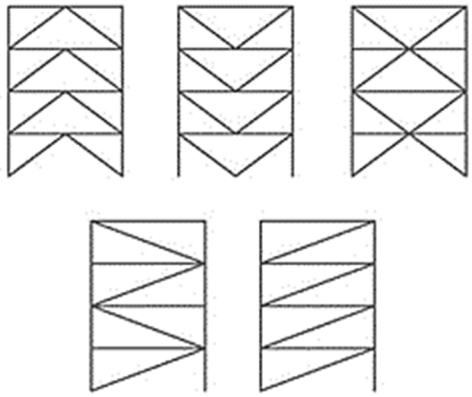

Fig. 2. Different BRBF configurations [AISC 341-16]

This symmetrical behavior results from restrained buckling of steel core in bracing elements. Moreover, axial load applied on the steel core is restrained; in buckling resistance mechanism casing usually resists against total core buckling and restrains steel core buckling in higher modes.

In BRBF system, bracing elements absorb energy in tension yield-symmetrical pressure cycles. Fig. 3 shows residual curve of this type of brace compared with typical braces.

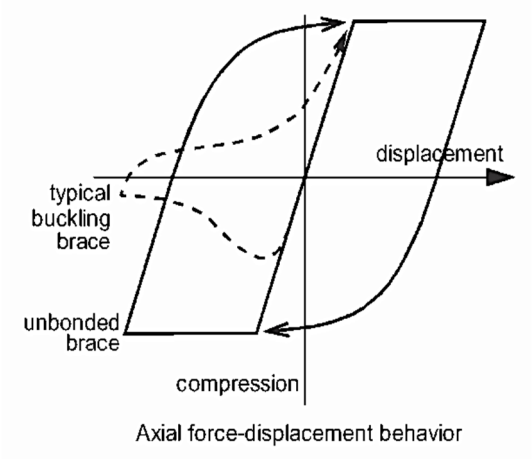

Fig. 3. BRBF behavior compared with typical brace (courtesy of Seismic Isolation Engineering) [AISC 341-16]

Generally, BRBF can provide so elastic stiffness that it can be compared with CBF. Laboratory results with real dimensions show that correct details and design of BRBF elements exhibit symmetric hysterical behavior under compressive and tensile forces during non-elastic deformations, so that ductility and energy dissipation of BRBF are expected to be comparable with special moment frame (SMF) and higher than SCBF. This high ductility results from restrained steel core buckling.

3.2. Characteristic parameters of buckling restrained brace

To ensure practical behavior, it is necessary to test braces. Testing of buckling restrained braces is explained in section F.4 of AISC 341-16 code. From these tests, maximum forces applied by braces on the system will be obtained. These maximum forces are used for analysis required in section F4.3. Fig. 6 shows bilinear diagram of force-displacement relationship. Compressive strength adjustment factor, β, and strain hardening adjustment factor, ω, depend on bracing forces and nominal yield strength of materials. This is pointed out in recent experiments on buckling restrained braces.

3.2.1. Compression Strength Adjustment Factor (β)

Compressive strength adjustment factor (β) calculates additional compressive strength (considering tensile resistance) and it is defined as:

$$\beta = \frac{\beta\omega F_{ysc}A_{sc}}{\omega F_{ysc}A_{sc}} = \frac{P_{max}}{T_{max}} \quad (1)$$

3.2.2. Strain Hardening Adjustment Factor (ω)

Strain hardening adjustment factor (ω) defined as:

$$\omega = \frac{\omega F_{ysc}A_{sc}}{F_{ysc}A_{sc}} = \frac{T_{max}}{F_{ysc}A_{sc}} \quad (2)$$

Where:
A_{sc}: cross-sectional area of the yielding segment of steel core (mm²)
F_{ysc}: measured yield strength of the steel core (MPa)
P_{max}: maximum compression force (N)
T_{max}: maximum tension force within deformations corresponding to maximum 200% of the design story drift (these deformations are defined as $2\Delta_{bm}$) or 2% of the floor height.

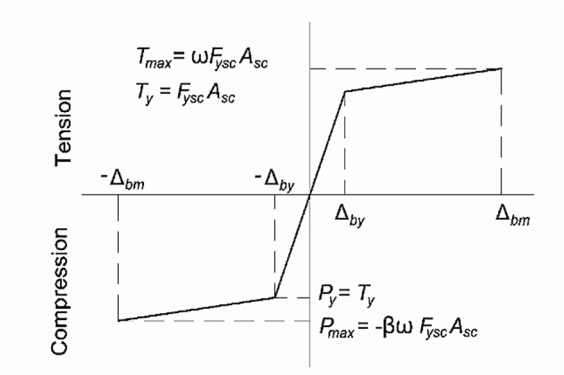

Fig. 4. Displacement-force diagram [AISC 341-16]

3.2.3. Cumulative inelastic deformation (CID)

Cumulative inelastic deformation (explained in section K.3 of AISC 341-16 code) is obtained by dividing brace deformation by displacement of story to brace yield deformation.

$$CID = \frac{\Delta_p}{\Delta_{by}} \quad (3)$$

Δ_p: brace deformation by displacement of story
Δ_{by}: displacement in yield point

$$\Delta_p = \frac{E_h}{P_y} \quad (4)$$

E_h: area of each loop of hysteresis curve
P_y: average value of effective yield force

$$P_y = \omega P_{yn} \quad (5)$$

P_{yn}: core nominal yield force

$$P_{yn} = F_{yn}A_{sc} \quad (6)$$

F_{yn}: core nominal yield strength

3.3. Previous models

The first BRB was designed by Kimura et al in which a typical brace coated by steel pipe filled by mortar was used. In this study, several stable hysterical characteristics were considered and reported; by continuing compressive loading cycle, this led to vertical deformation of mortar to a large cavity which was adequate to start local buckling during correct compressive loading.

Mochizuki et al, (1980) conducted experiments on similar braces in which its adhesion to internal brace was prevented by a concrete. This study showed that the concrete was cracked and its buckling-restraining effect decreased under cycling loading. A decade later, buckling restrained braces shown in Fig. 5 were developed by Watanabe, Wada, and Nakamura.

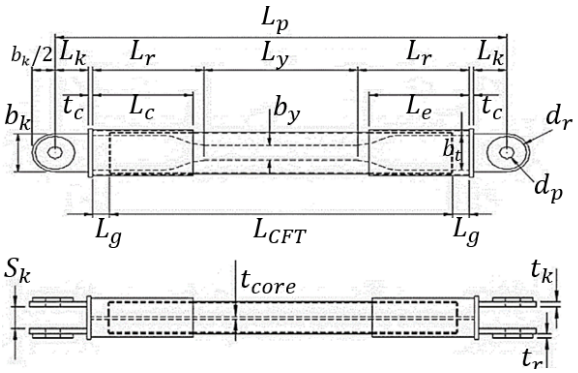

Fig. 5. General BRB configuration

Chae et al. (2004) conducted studies on feasibility of direct displacement method on damage tolerant brace frame (DTBF) with joint beam-column joints. Moreover, two seismic records were developed from UBC 97 based on design spectrum and were used in analyzing nonlinear time history on 3 and 5-story buildings. The results showed that axial forces and bending moments applied on columns of a low-rise structure were not considerable; this implied the philosophy of damaged tolerant structure. For example, BRBs dissipate fluctuating energy of inelastic deformation, while other structural elements remain elastic without damage. The suggested design method was more accurate than energy balance theory in which hysterical energy was dissipated by BRB and was not estimated in approximate formula suggested by Housner, but was directly obtained from hysteric energy spectrum developed by a series of time history analyses.

Elnashai and Sarno, (2009) evaluated seismic performance of moment resistant frames (MRF) reinforced by different bracing systems in three structural configurations including SCBF, BRBF, and MBF. They designed a 9-story building with peripheral steel MRF and insufficient lateral stiffener to satisfy drift constraints of the code in highly seismic areas. Then, the frame was reinforced by SCBFs, BRBFs, and MBFs and inelastic time history analysis was studied to evaluate structural performance and local (member rotations) deformations and total deformations (ceiling and inter-story drift) under earthquake.

Wigle and Fahnestock, (2010) developed a nonlinear finite element model to study BRBF beam-column joints and validated it by a previously tested empirical sample. They also evaluated parametric studies on different joint configurations to assess key factors of effective performance and it was concluded that joint configuration has a significant effect on general response of the system and local joint demand.

4. Sample Desing, Construction and Testing

For the predicted procedure of this study, a solved problem in (Walterio and Sabelli, 2004). According to laboratory constraints, maximum sample length was set at 2m for the experiment, while the real sample (braced frame in story 2, BF-2) was about 5.6m in length. For equal tension in the laboratory sample and prototype, scale decrement factor was set at 0.358 for length and 0.128 for area. This study tended to construct this brace to tolerate forces applied on it based on AISC 341-16.

Buckingham Pi Theorem is the accepted basis for performing dimensional analysis. *N* number of physical variables that are represented by *K* basic units can be translated from their original form into (*N–K*) non-dimensional variables, known as Π terms. This reduces the number of independent variables to be experimentally validated for a given problem. Because each Π term is dimensionless, they can be used as a general tool to equate model and prototype behavior. Scale modelling using these Π terms requires that the following be true:

$$\Pi_i^{(m)} = \Pi_i^{(p)} \; for \; i = 1,2,3,\dots(N-K) \tag{7}$$

Through a real experiment, (Fahnestock et al, 2003) used this size reduction for their experiments. The prototype (p) was simulated to laboratory model (m) at 0.358 scale as follow and forces applied on BRB are listed in Table 1.

$$\lambda = \frac{L_m}{L_p} \tag{8}$$

$$\lambda = \frac{2}{5.6} = 0.358$$

$$\sigma_m = \sigma_p \Rightarrow \frac{F_m}{A_m} = \frac{F_p}{A_p} \Rightarrow \frac{F_m}{F_p} \times \frac{A_p}{A_m} = 1 \tag{9}$$

$$\lambda^2 = \frac{A_m}{A_p} \tag{10}$$

λ^2 = 0.128

$\frac{F_m}{F_p}$ = 0.128

$\frac{\varepsilon_m}{\varepsilon_p}$ = 1

L_m: brace length in laboratory model

L_p: brace length in prototype

σ_m: brace stress in laboratory model

A_m: brace area in laboratory model

A_p: brace area in prototype

F_m: brace force in laboratory model

F_p: brace force in prototype

ε_m: brace strain in laboratory model

ε_p: brace strain in prototype

Table1. Forced applied on BRB

	Effective length (L) (m)	Axial force (P_u) (ton)
Prototype	5.6	153.13
Laboratory model	2	19.6

For the laboratory *model, we can write:*

$$\varphi P_n = \varphi P_{ysc} = \varphi F_{ysc} A_{sc} \quad (11)$$

$$0.9 \times 2672\left(\frac{\text{kg}}{\text{cm}^2}\right) \times 8.6(\text{cm}^2) = 20.68 \text{ ton}$$

$$DCR = \frac{P_u}{\varphi P_n} \quad (12)$$

$$\frac{19.6}{20.68} = 0.95 < 1.00$$

$$\Delta_{bx} = \frac{P_{bx} L_{ysc}}{E A_{sc}} \quad (13)$$

L_{ysc} = BRB yield length.

This length is about 2/3 of the length of the work point in the diagonal brace and half the length of the work points in the chevron brace (Fig. 6).

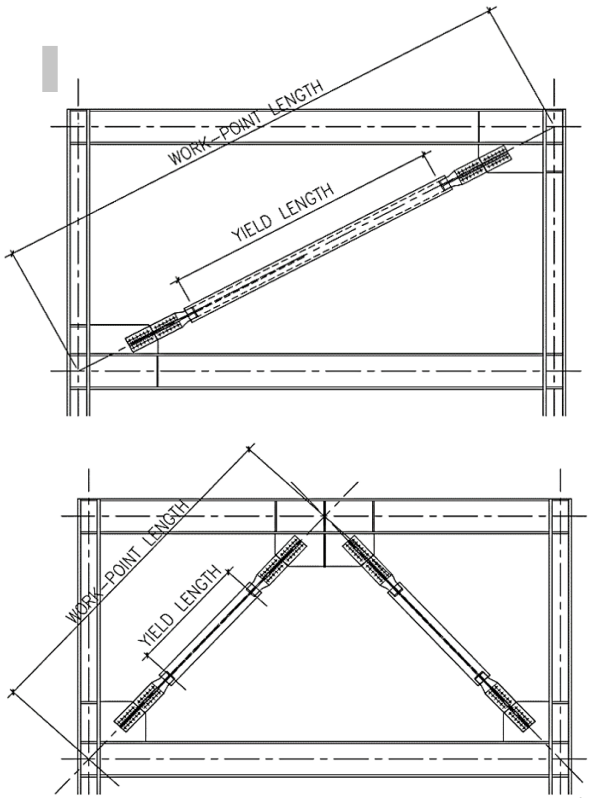

Fig. 6. BRB yield length

Δ_{bx} = 0.08cm

$$\Delta_{bm} = C_d \, \Delta_{bx} \quad (14)$$

Δ_{bm} = 0.4cm

$$\varepsilon_{BRB} = \frac{2\,\Delta_{bm}}{L_{ysc}} \quad (15)$$

ε_{BRB} = 0.8%

4.1. BRB map

Based on above calculations, the execution map was designed considering screw-welding end joint, core cross-section A_{sc}=8.6(cm²), made by steel A36, yield tension 2672(kg/cm²), as shown in Fig. 7-9. Required parameters of the experiment are as follows:

$P_{ysc} \geq F_{ysc} \, A_{sc}$ = 3234(kg/cm^2) × 8.6(cm^2) = 27.8 ton

$\varepsilon_{BRB} \geq$ 0.8%

$$\Delta_y = \frac{F_{ysc} L_{ysc}}{E} \quad (16)$$

considering E=2038902(kg/cm²) and F_{ysc}=3234(kg/cm²), we have:

Δ_{by} = 0.16cm

Δ_{bx} = 0.08cm

$2\Delta_{bm}$ =0.8cm

Tables 2 and 3 list characteristics of BRB core plate.

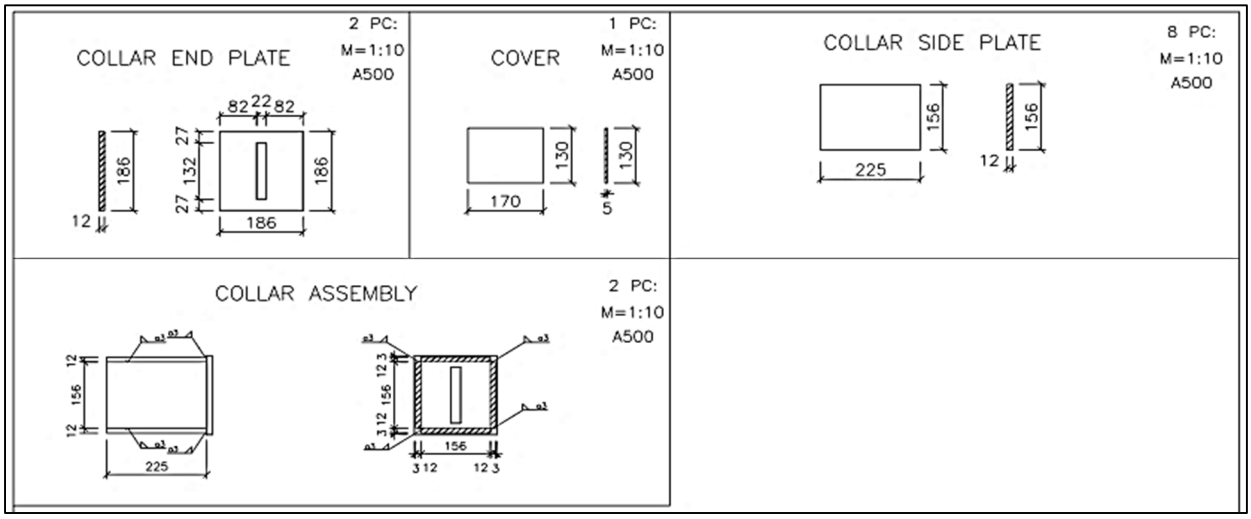

Fig. 7. Details of core and casing

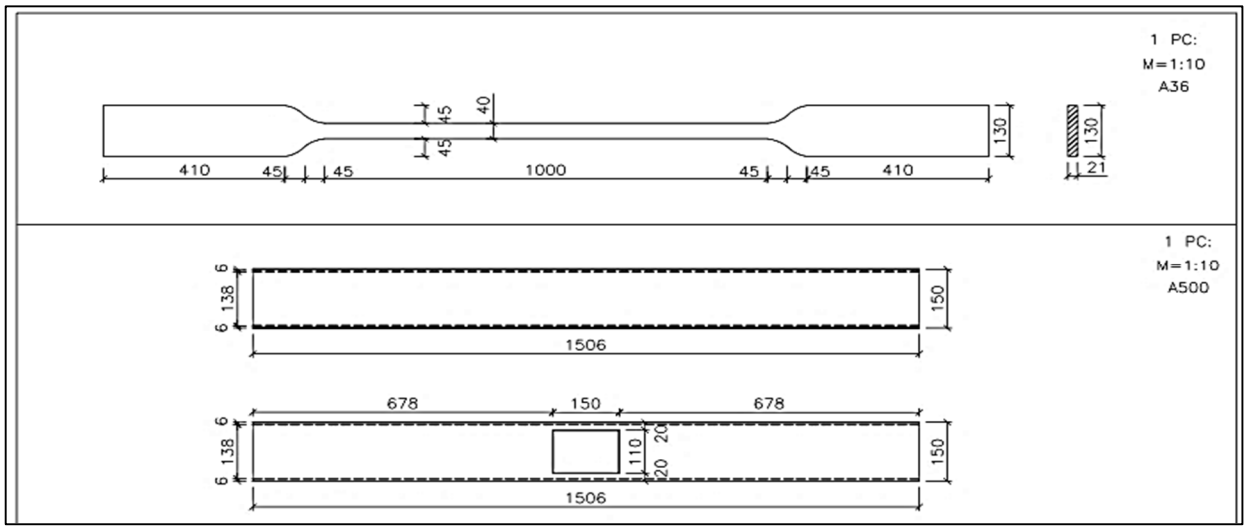

Fig. 8. Shear details of plates

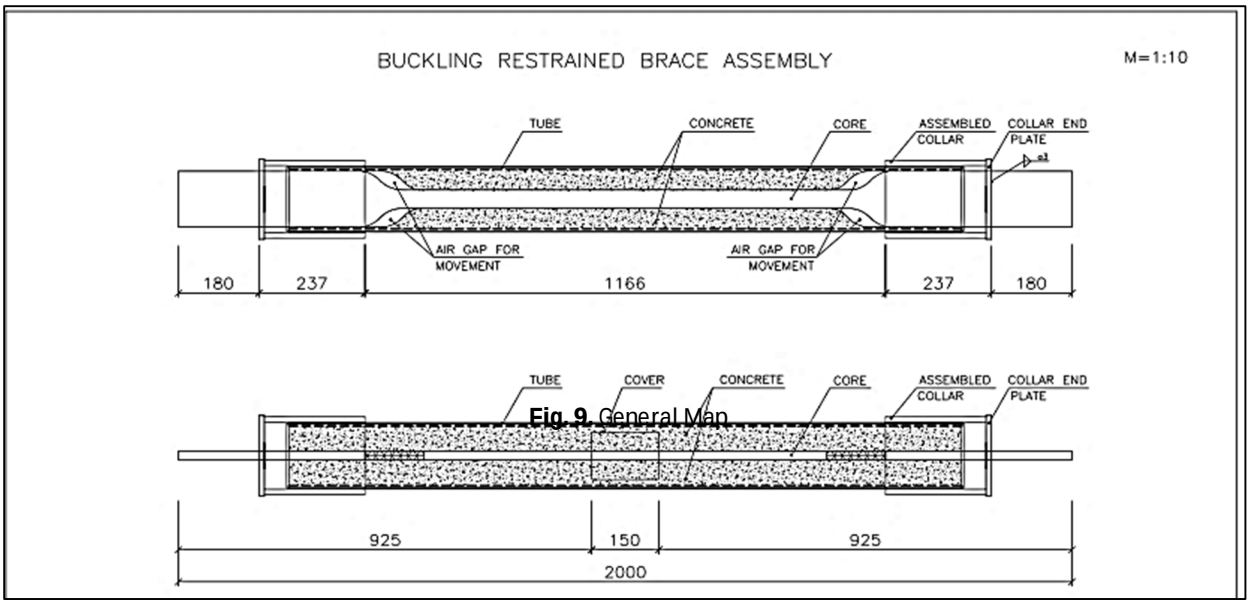

Fig. 9. General Map

Table 2. Characteristics of BRB core plate

Brace Designation			PC (1) or WC(2)
Specified yield strength, F_y (kg/cm²)			2672
# of Plates			1
Core of Plate		Thickness (t_p) (cm)	2
		Total Thickness (t_r) (cm)	2
	Elastic Zone (EZ)	Width (b_{EZ}) (cm)	13
		Length (L_{EZ}) (cm)	23.7
		Stiffness (K_{EZ}) (kg/cm²)	2,236,770
	Transition Zone (TZ)	Width (b_{TZ}) (cm)	13
		Length (L_{TZ}) (cm)	9
		Stiffness (K_{TZ}) (kg/cm²)	5,890,161
	Yielding Zone (YZ)	Width (b_{YZ}) (cm)	4.3
		Length (L_{YZ}) (cm)	100
		Stiffness (K_{YZ}) (kg/cm²)	175,346

(1) PC: Pin Connection
(2) WC: Weld Connection

Table 3. Characteristics of BRB core plate

Brace Designation	Yield Force (P_y) (kgf)	Deformation at first significant yield (cm)			
		Elastic Zones	Transition Zone	Yielding Zone	Total Brace
WC or PC	22979.2	Δ_{EZ}	Δ_{TZ}	Δ_{YZ}	Δ_{by}
		0.021	0.008	0.131	0.16

4.2. Loading Protocol

Based on requirements of the K.3 section of the code AISC 341-16 loading protocol is considered. Table 4 describes loading protocol.

4.3. Sample Construction

Although yield tension of steel core was set at 260(kg/cm²), two tensile tests were done on the processed materials and the mean 2790(kg/cm²) was considered for yield tension, based on which its design was modified as follow. For the laboratory model, we have:

$$\varphi P_n = \varphi P_{ysc} = \varphi F_{ysc} A_{sc}$$

$$= 0.9 \times 2790(\text{kg/cm}^2) \times 8.4(\text{cm}^2) = 21.09 \text{ ton}$$

$$DCR = \frac{P_u}{\varphi P_n} = \frac{19.6}{21.09} = 0.93 < 1.00$$

$$\Delta_{bx} = \frac{P_{bx} L_{ysc}}{E A_{sc}} = 0.08\text{cm}$$

$$L_{ysc} = 0.5L = 100\text{cm}$$

$$\Delta_{bm} = C_d \, \Delta_{bx} = 0.4\text{cm}$$

$$\varepsilon_{BRB} = \frac{2\,\Delta_{bm}}{L_{ysc}} = 0.8\%$$

Therefore, core cross-section was changed from 8.6(cm²) to 8.4(cm²) and new maps were designed considering screw-weld end joint, core cross-section A_{sc}=8.4(cm²), made by steel A36, yield tension 2790(kg/cm²). Required parameters for the test include:

$$P_{ysc} \geq F_{ysc} \, A_{sc} = 2970(\text{kg/cm}^2) \times 8.4\left(\text{cm}^2\right) = 23.4 \text{ ton}$$

$$\varepsilon_{BRB} \geq 0.8\%$$

$$\Delta_y = \frac{F_{ysc} L_{ysc}}{E}$$

considering E=2038902(kg/cm²) and F_{ysc}=3234(kg/cm²), we have:

$$\Delta_{by} = 0.16\text{cm}$$

$$\Delta_{bx} = 0.08\text{cm}$$

$$2\Delta_{bm} = 0.8\text{cm}$$

Table 5 lists BRB characteristics.

Characteristics of the required materials are presented in Table 6.

4.3. Sample construction

Although yield tension of steel core was set at 260(kg/cm²), two tensile tests were done on the processed materials and the mean 2790(kg/cm²) was considered for yield tension. (Table7) based on which its design was modified as follow. For the laboratory model, we have:

$$\varphi P_n = \varphi P_{ysc} = \varphi F_{ysc} A_{sc}$$

$$= 0.9 \times 2790(\text{kg/cm}^2) \times 8.4(\text{cm}^2) = 21.09 \text{ ton}$$

$$DCR = \frac{P_u}{\varphi P_n} = \frac{19.6}{21.09} = 0.93 < 1.00$$

$$\Delta_{bx} = \frac{P_{bx} L_{ysc}}{E A_{sc}} = 0.08\text{cm}$$

$$L_{ysc} = 0.5L = 100\text{cm}$$

$$\Delta_{bm} = C_d \, \Delta_{bx} = 0.4\text{cm}$$

$$\varepsilon_{BRB} = \frac{2\,\Delta_{bm}}{L_{ysc}} = 0.8\%$$

Table 4. Loading Protocol

	STEP	1	2	3	4	5	6	7
AISC	Cycles	2	2	2	2	2	As needed	
	Δ_b/Δ_{by}	1.00	2.50	5.00	7.50	10.00	7.50	
WC	Cycles	6	4	6	4	2	2	2
	Δ_b (cm)	0.20	0.50	1.01	1.48	1.88	2.35	2.82
	Δ_b/Δ_{by}	1.25	3.13	6.31	9.25	11.75	14.69	17.63

Table 5. BRB Characteristics

WC series-sample length of 2(m)	A_{sc} (cm²)	F_y (kg/cm²)	Δ_b/Δ_y	P_y (ton)	P_u (ton)	CID	β
WC Brace 1	1×4.3×2=8.6	2876	10	23	36	140	1.16
Loading speed: 0.635 (mm/s)							

Table 6. Materials required to build a welded BRB sample

Steel casing	Height	Width	Thickness	Length	Weight per meter	Total weight
	d	b	t	l		
	cm	cm	cm	cm	kg	kg
	15	15	0.6	150	27.1	41

Core plate	transition zone		yielding zone				
	Length	Width	Length	Width	Thickness	Number of cores	Total weight
	L_{tz}	b_{tz}	L_{yz}	b_{yz}	t_{cp}		
	cm	cm	cm	cm	cm	-	kg
	0	0	200	15	2	1	47

Plate	end plate				knife plate				
	Length	Width	Thickness	Number	Length	Width	Thickness	Number	Total weight
	L_{ep}	b_{ep}	t_{ep}	-	L_{kp}	b_{kp}	T_{kp}	-	kg
	cm	cm	cm	-	cm	cm	cm	-	
	19	19	1.2	2	0	0	0	0	7

Collar	Collar					
	Length	Height	Width	Thickness	Number	Total weight
	L_{co}	h_{co}	b_{co}	t_{co}	-	kg
	cm	cm	cm	cm	-	
	23	16	16	1.2	4	28

Table 7. Steel core strength

yield strength, F_y (kg/cm²)	2790
ultimate strength, F_y (kg/cm²)	4100

Table 9. Modified steel core characteristics; Yield deformation for braces (Δ_{bm}=0.8cm)

Brace Designation	Yield Force, P_y (kg)	Deformation at first significant yield				Unit
		Elastic Zones, Δ_{EZ}	Transition Zone, Δ_{TZ}	Yielding Zone, Δ_{YZ}	Total Brace Δ_{by}	
WC	23436	0.034	0.012	0.137	0.183	cm
		0.34	0.12	1.37	1.83	mm

Table 10. Modified loading protocol

	STEP		1	2	3	4	5	6	7
ALTIN	AISC	Cycles	2	2	2	2	2	2	As needed
	Δ_b/Δ_{bm}	Δ_{by}	0.50	1.00	1.50	2.00	2.50	3.00	
BRB-01	Δ_b (cm) According to the calculations		0.18	0.50	1.01	1.48	1.88	2.35	2.82
	Δ_b (cm) Implemented in loading		0.23	0.58	1.15	1.69	2.15	2.69	3.23

Therefore, core cross-section was changed from 8.6(cm²) to 8.4(cm²) and new maps were designed considering screw-weld end joint, core cross-section A_{sc}=8.4(cm²), made by steel A36, yield tension 2790(kg/cm²).

Required parameters for the test include:

$P_{ysc} \geq F_{ysc}\, A_{sc}$ = 2970(kg/cm²) × 8.4(cm²) = 23.4 ton

BRB length = 200cm

ε_{BRB} =≥ 0.8%

axial deformation: $\Delta_y = \frac{F_{ysc} L_{ysc}}{E}$

Now, considering E=2038902kg/cm² and F_{ysc}=2790kg/cm², we have:

Δ_{by}=0.16cm

Δ_{bx}=0.08cm

By modifying the results obtained by changing yield tension and applying it on the execution maps shown in Fig. 10-12, the core plate was cut by CNC device and got ready for assembly after pilling and modifying potential distortions caused by cooling.

Fig. 10. Core cutting

Then, steel casing was cut in the considered sizes to assembly two ends of the can vertically. Now, steel plates of the collar were cut by guillotine and CNC for assembly. Then, both collar parts were welded and assembled to the considered areas after adjusting plates.

The steel core could now be placed and stabilized in the steel casing. Considering the sensitivity of placing steel core within the considered location, this was done very cautiously. Finally, the pieces were assembled and welded cautiously by using the electrode 6013. Then, the chips on the piece were removed by a wired brush. The sample was concreted, stained and tested. Resistance was about 600(kg/cm²) for seven days.

4.4. Sample testing

By cooperation of the International Institute for Earthquake, the designed experiment was done in structural laboratory of the institute. Requirements of the Code AISC 341-16 regarding BRB experiment are as follows:

- Hysteresis curve show stable and repetitive behavior;
- Brace should not be unstable and fractured or have disrupted end joint;
- For axial experiments, maximum tensile and compressive forces should not be smaller than nominal resistance of the core in a cycle in which deformation is larger than Δ_{by};
- For axial experiments, the ratio of maximum compressive force to maximum tensile force (β) should not exceed 1.3 in a cycle in which deformation is larger than Δ_{by};
- For braces under axial force, η or cumulative inelastic deformation should be at least 140.

Fig. 11 shows assembly steps in UTM. Fig. 12 shows hysteresis curve. Fig. 13 shows loading protocol of the sample.

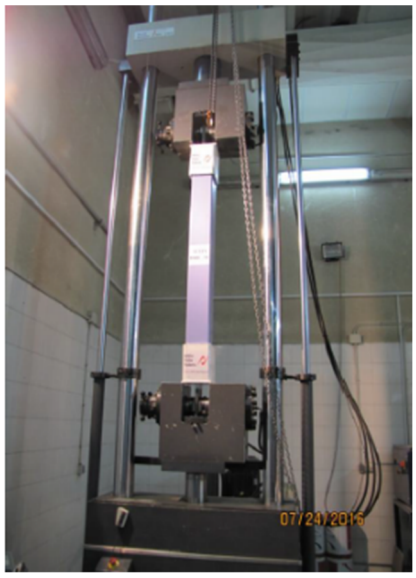

Fig. 11. Implementation and assembly of sample in structural laboratory

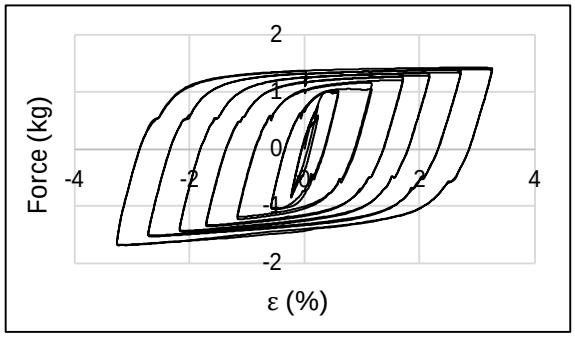

Fig. 12. Hysteresis curve of the sample

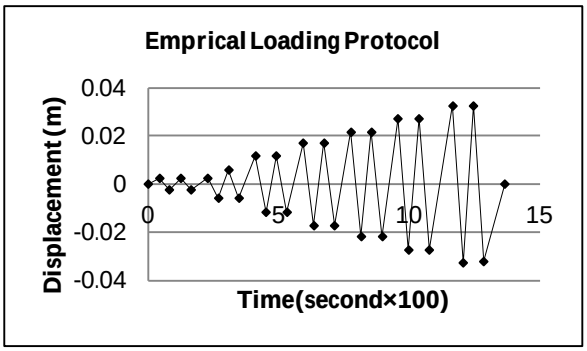

Fig. 13. Empirical loading protocol

5. Numerical Modelling

The present numerical study was conducted based on the results of previous paragraph by support of the Science and Technology Park of East Azarbaijan province. For faster convergence, static pushover method was used for finite element modelling. Linear geometric deformation theory which refers to rotations and strains is assumed very small.

5.1. Steel core

Steel core shown in Fig. 14 plays a very important role in buckling performance of the buckling restrained brace. In core analysis in which steel A36 was used to increase ductility and energy dissipation, eight-node three-dimensional cubic element was used for modelling.

Fig. 14. Core model

5.2. Concrete casing

According to Fig. 15, concrete casing provided a continuous support which prevents core buckling. In this casing, Young module of concrete was 21(GPa) and Poisson ratio was 0.18. Due to complex modelling, a number of partitions were used to simplify meshing.

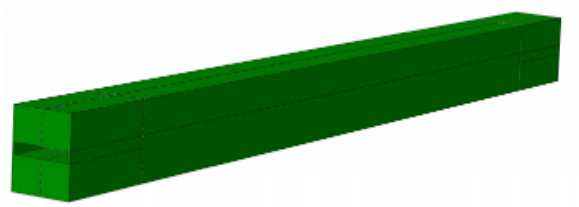

Fig. 15. Concrete casing

According to Fig. 16, material layer (here, air gap) was used between steel core and concrete casing to provide a space for transverse displacement, in which different buckling modes start. This empty space is 50mm between steel core transmission zone and concrete casing to start buckling

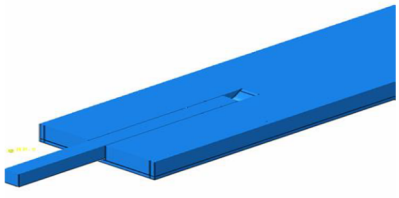

Fig. 16. Empty space

5.3. Steel tube

According to Fig. 17, steel prism with empty square-shaped can section was used for steel tube. For continuity and better description of contact surface between concrete casing and steel tube, three-dimensional rigid element was used instead of continuous element.

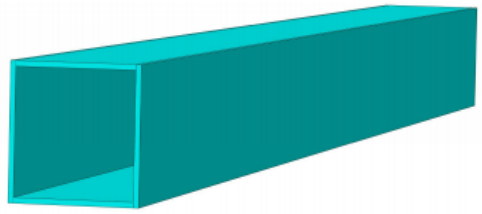

Fig. 17. Steel Casing

5.4. Full model

Full model including steel casing, steel core, and steel tube is shown in Fig. 18. The lower part of steel core provides welding joint to connect plates. Tie constraints allow the tube and concrete interact with steel core.

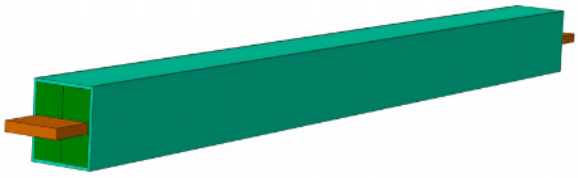

Fig. 18. Full BRB model

5.5. Determine mesh density

In finite element analysis, mesh is the main component; if the model is complex, costs can be significantly reduced by using partitioning and meshing techniques. Different mesh sizes and the type of element influence convergence, time and accuracy. Large sizes of element reduce time and

cost of calculations, while small size of element increases the accuracy of results, but increases cost of calculations and time of modelling. Therefore, proper mesh size is very important to balance these approaches for obtaining accurate results. Fig. 19 shows meshing of the full model.

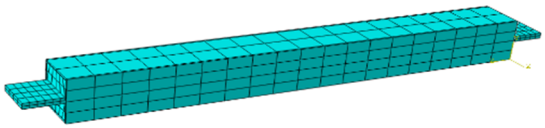

Fig. 19. General meshing

5.5. Gap size

In empirical experiment, it is important to ensure that axial element performs independently from yield of steel core and casing. Therefore, proper non-adhesive materials can prevent the concentration of tension resulting from core-enclosing system adhesion; ignoring this can lead to non-uniform distribution of yielding and early local buckling. Therefore, it is essential to consider non-adhesive air gap between the core and casing in finite element modeling. The gap provides sufficient space for free lateral expansion of core plate and reduction of friction response as well as regulation percent of compressive resistance. However, larger gap can lead to undesirable performance; when the gap is very smaller than 0.2 mm, the steel core may not have sufficient space for expansion in pressure and concrete will be involved with steel core under greater strains. Moreover, if the gap size is very large, casing will not enclose steel core, which leads to the loss of enclosing function of the core and transmission of loads. Both conditions should be avoided considering suitable gap sizes around the steel core. Symmetrical hysteresis curve will be obtained by selecting suitable gap sizes.

5.6. Friction coefficient

Another important characteristic is friction between yielding core and concrete casing; by selecting suitable non-adhesive materials, tension concentration resulting from adhesion and connection between the core and enclosing system, which leads to non-uniform distribution of yielding, can be avoided. Non-uniform distribution of yielding leads to early local buckling and fatigue in lower cycle. This section evaluates the effect of friction coefficient and runs finite element modelling through rigid contact (restraining relative movements to slip) in which both surfaces are placed within very rigid springs, node to node, in the finite element.

If friction coefficient is smaller than 0.15, it does not influence hysteresis cycle; however, it increases maximum compressive load and hysteresis curves are stable, resulting in almost symmetrical force by reasonable increase in maximum compressive load. When friction coefficient changes from 0.15 to 0.3, it leads to instable hysteresis curves, resulting in asymmetry by acceptable increase in maximum compressive load. In this modelling, friction coefficient is set at 0.1.

Another characteristic is lateral deformation. When friction between core and concrete is small enough, lateral deformation is almost symmetrical along the core in the middle of the core length. When friction coefficient increases, lateral deformation becomes asymmetrical and peak movements go toward stable support, resulting in fluctuations near the fixed end which develop with lateral deformation. When friction coefficient is very large, it leads to an obvious jagged shape in cyclic response curve, because contacting core and concrete lead to development of greater friction forces in contact areas between core and concrete; this even occurs when the steel core is under pressure in higher modes. Moreover, this occurs when loading changes from pressure to tensile. Table 11 shows the characteristics of core steel and Table 12 shows its plastic characteristics.

Table11. Characteristics of core steel

Material-A36	
$f_{y,charecteristic}$=235Mpa	$f_{y,actual}$=279Mpa
$f_{u,charecteristic}$=360Mpa	$f_{y,actual}$=450Mpa
ρ=7850kg/m3	

Table12. Plastic characteristics of core steel

Cyclic hardening	
Kinematic hardening parameter (C)	Gamma(γ)
25000	500
21000	375
5950	120
935	25
300	0

5.7. Properties of concrete materials

Table 13 shows properties of casing concrete. Fig. 20 shows tie joint of concrete casing to steel casing.

Table13. Properties of casing concrete

E_0=210Gpa
E_c=210Gpa
ν=0.30
ν_c=0.18

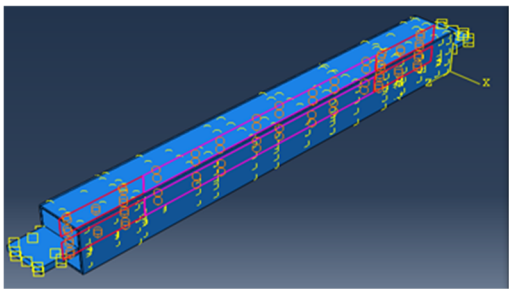

Fig. 20. Concrete casing joint to steel casing

5.8. Loading

Model loading as a cyclic protocol shown in Fig. 13 is applied on a steel core shown in Fig. 21.

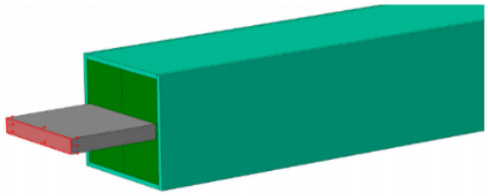

Fig. 21. Location of load applied

5.10. Support conditions

To define support conditions, steel core end is closed and its displacement and rotation are discarded.

5.11. Analysis results

Fig. 22 shows steel core deformation and Fig. 23 and 24 show support forces and model displacement, respectively.

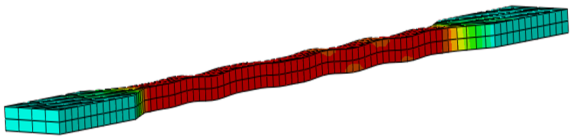

Fig. 22. Deformed steel core

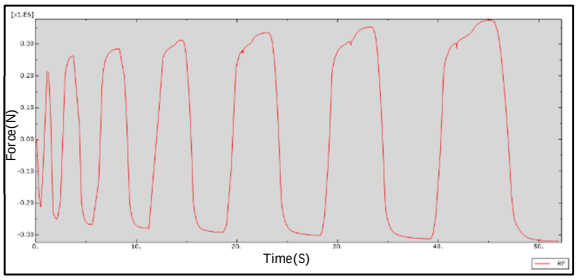

Fig. 23. Support forces

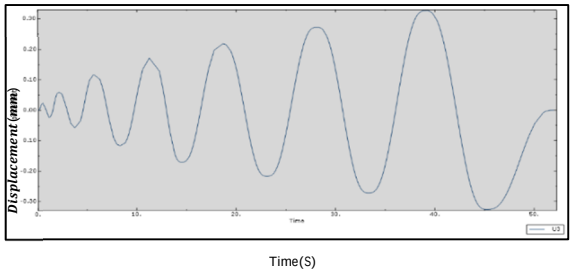

Fig. 24. Displacement

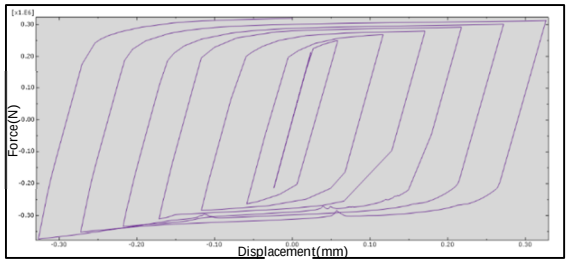

Fig. 25. Hysteresis curve of the numerical model

Fig. 25 and 26 show numerical and empirical hysteresis curves, respectively. Fig. 27 shows push comparison of hysteresis curves.

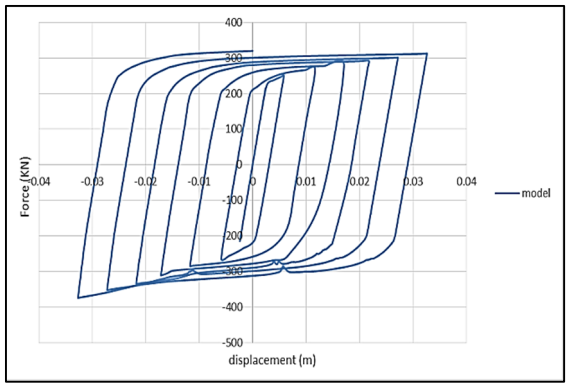

Fig. 26. Hysteresis curve of the empirical model

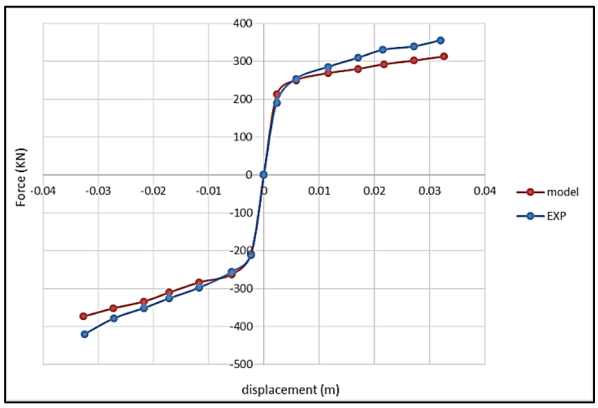

Fig. 27. Push comparison of numerical and empirical hysteresis curves

According to section K.3 of the code AISC 341-16 for axial experiments, the ratio of maximum compressive force to maximum tensile force (β) should not exceed 1.3 in a cycle in which deformation is larger than Δ_{by}. To estimate β, ω is first estimated from Fig. 28.

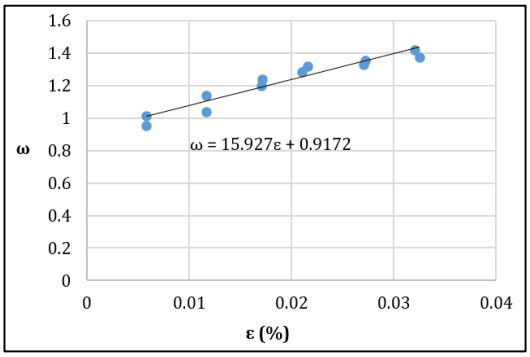

Fig. 28. Strain versus ω

Now, $\omega\beta$ is divided by ω to calculate β as shown in Fig. 29.

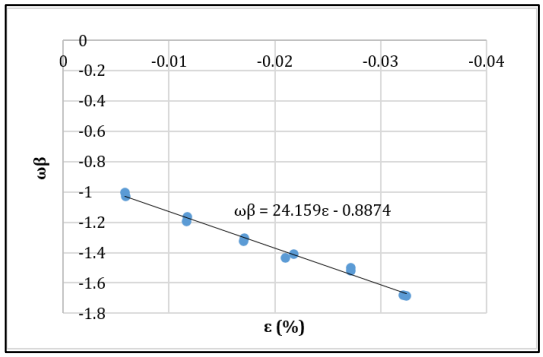

Fig. 29. Strain versus $\omega\beta$

Table 14 calculates β and $\omega\beta$.

Table14. Calculation of β

ε (%)	$\omega\beta$	ω	β
-0.00582	-1.00343	0.954996	1.05
-0.00584	-1.02609	1.0148	1.01
-0.01167	-1.16116	1.041136	1.12
-0.01166	-1.19084	1.141	1.04
-0.01704	-1.32215	1.197616	1.10
-0.01707	-1.30345	1.23672	1.05
-0.02096	-1.4331	1.284604	1.12
-0.02174	-1.40793	1.320184	1.07
-0.02715	-1.4973	1.329868	1.13
-0.02713	-1.51608	1.356548	1.12
-0.03212	-1.6773	1.376732	1.22
-0.03243	-1.68142	1.421964	1.18

According to Table 14, β is smaller than 1.3 for all strains and yield strain. Accordingly, the section K.3 of the code AISC 341-16 can be controlled for braces exposed to axial force; based on this code, cumulative inelastic deformation (CID) should be at least 140.

According to equation (3-4) we have:

$$\Delta_p = \frac{E_h}{P_y} = \frac{4798(\text{ton.cm})}{25.4(\text{ton})} = 188.82(\text{cm})$$

$$\text{CID} = \frac{\Delta_p}{\Delta_{by}} = \frac{188.82(\text{cm})}{0.38(\text{cm})} = 497$$

It can be observed that CID is larger than 140 (the least determined by AISC). Finally, for maximum strain (3.2%), we have:

ω=1.33 β=1.13 CID=497

Obviously, the brace can respond to forces and design strain ε=0.8%; according to AISC, the results of axial experiment meet all requirements of AISC.

6. Conclusion

Hysteresis curve resulting from the experiment shows stable, symmetrical behavior and the ability to adopt suitable cycles. Exact evaluation of the sample showed no instability and fracture in the brace.

For all displacements larger than Δ_{by}, maximum tensile and compressive forces are larger than 21(ton). For all strains and yield strain, β is smaller than 1.3. CID is larger than 140 (the least determined by AISC). This study determined empirical parameters of design and localized BRB.

Finite element modelling was reasonably consistent with laboratory studies and hysteresis curve of the tested brace showed a stable, repetitive behavior by increasing stiffness. No instability and failure was observed in the experiment process. According to requirements of the code AISC 341-16, β and ω were larger than 1 and β was smaller than 1.3; moreover, CID was larger than 140. As the Code 2800 requires to use BRBF which performed well in a 9 Richter earthquake in Japan in 2011, leading to higher confidence to AISC 341, BRBF can be an economic and practical alternative for conventional systems due to its simple design and easy implementation.

References

AISC341-16, "Seismic provisions for structural steel buildings", Chicago: American Institute of Steel Construction, 2016.

Kersting RA, Fahnestock LA, Lopez WA, "Seismic design of steel buckling-restrained braced frames: a guide for practicing engineers", NEHRP Seismic Design Technical Brief, 2015, 11, NIST GCR 15-917-34.

Sabelli R, Lopez W, Steel tips: "Design of buckling-restrained braced frames", Structural Steel Educational Council, 2004.

Christopher Ar, Fahnestock LA, "Evaluation of buckling-restrained braced frame seismic performance considering reserve strength", Journal of Engineering Structures, 2011, 33 (1), 77-89.
https://doi.org/10.1016/j.engstruct.2010.09.020

Sabelli R, Stephen M, Chunho, "Seismic demands on steel braced frame buildings with buckling-restrained braces", Engineering Structures, 2003, 25 (5), 655-666.
https://doi.org/10.1016/S0141 0296(02)00175-X

Kimura I, Hidetsugu H, "Process of manufacturing whisker crystalline silicon carbide", U.S. Patent 20 Jan. 1976, 3, 933,984.

Mochizuki N, "An experimental study on buckling of unbonded braces under centrally applied loads", Proc. Annual Meeting of the Architectural Institute of Japan,1980.
https://doi.org/10.1016/j.jcsr.2019.04.042

Chae BG, Ichikawa Y, Jeong GC, Seo YS, Kim BC "Roughness measurement of rock discontinuities using a confocal laser scanning microscope and the Fourier spectral analysis", Engineering Geology, 2004, 72, 3-4, 181-199.
https://doi.org/10.1016/j.enggeo.2003.08.002

Wigle Victoria R, Fahnestock LA, "Buckling-restrained braced frame connection performance", Journal of Constructional Steel Research, 2020, 66 (1), 65-74. https://doi.org/10.1016/j.jcsr.2009.07.014

Di Sarno L, Elnashai AS, "Bracing systems for seismic retrofitting of steel frames", Journal of Constructional Steel Research, 2009, 65 (2), 452-465.
https://doi.org/10.1016/j.jcsr.2008.02.013

Lopez WA, Sabelli R, "Seismic Design of Buckling Restrained Braced Frames", DASSE Design, Inc., US, 2004.

Uang CM, Nakashima M, Tsai KC, "Research and application of buckling restrained braced frames", International Journal of Steel Structure, 2004, 4, 301-13.

Takeuchi T, Ida M, Yamada S, Suzuki K, "Estimation of cumulative deformation capacity of buckling restrained braces", Journal of Structural Engineering, ASCE 2008, 134, 822-831.
https://doi.org/10.1061/(ASCE)07339445(2008)134:5(822)

Sabelli R, Mahin S, Chang C, "Seismic demands on steel braced frame buildings with buckling-restrained braces", Engineering Structures, 2003, 25, 655-666.
https://doi.org/10.1016/S0141-0296(02)00175-X

Gholhaki M, Pachideh G, Lashgari R, Rezayfar O, "Experimental and numerical study of buckling restrained bracing behavior with combined steel and polyamide sheath", Iranian Society of Structural Engineering, 2013, 5 (4), 88-108.
https://doi.org/10.22065/jsce.2017.86109.1190

Tabatabaie A, Mirghaderi R, Hosseini A, "Experimental and numerical developing of reduced length buckling restrained braces", Engineering Structures, 2014, 77, 143-160.

Eryasar ME, "Experimental and Numerical investigation of buckling restrained braces", [Master of Science in Civil Engineering]: Middle East Technical University; 2009.

Dehghani M, Tremblay R, "Standard dynamic loading protocols for seismic qualification of BRBFs in eastern and western Canada", In: Proceeding of 15th world conference on earthquake engineering. Lisbon, Portugal: International Association for Earthquake Engineering, 2012.

Tremblay R, Poncet L, Bolduc P, Neville R, DeVall R, "Testing and design of buckling restrained braces for Canadian application", In: Proceeding of 13th world conference on earthquake engineering, 2004.